American Mineralogist, Volume 90, pages 1325–1334, 2005

A high-temperature diffraction study of the solid solution $CaTiOSiO_4$-$CaTiOGeO_4$

RIKKE ELLEMANN-OLESEN AND THOMAS MALCHEREK*

Mineralogisches Institut, Universität Heidelberg, Im Neuenheimer Feld 236, D-69120 Heidelberg, Germany

ABSTRACT

The structure of $CaTiOGeO_4$ (CTGO) has been refined using single crystal X-ray diffraction data. CTGO is isostructural with titanite, $CaTiOSiO_4$. The displacive $P2_1/a$-$A2/a$ phase transition analogous to titanite has been studied by in situ heating X-ray powder diffraction and transmission electron microscopy. The transition is accompanied by the disappearance of superstructure reflections, $k + l = 2n + 1$, which are replaced by diffuse scattering for $T > T_c$. The diffuse scattering is seen as streaks along **b*** in high-temperature TEM SAD. Lattice parameters as a function of temperature and composition were determined by X-ray powder diffraction between room temperature and a maximum of 1123 K. Strain analysis of CTGO indicates a transition temperature of $T_c = 588 \pm 4$ K and the additional occurrence of an isosymmetric anomaly at $T_i = 800 \pm 25$ K. There is complete solid-solution along the join $CaTiO(Ge_xSi_{1-x})O_4$. The lattice parameters across the solid solution vary continuously and the structural phase transitions were identified based on the determination of spontaneous strain associated with the transitions. The e_{11} and e_{13} components dominate the strain tensor. All compositions across the solid solution exhibit close to tricritical behavior and nearly constant scalar strain.

INTRODUCTION

The titanite structure has attracted substantial interest because of its phase transitions, its occurrence as a metamict mineral (Hawthorne et al. 1991), and its crystal chemical relation to the non-linear optical material $KTiOPO_4$ (KTP) (Kunz et al. 2000). Titanite is a common accessory mineral in a variety of metamorphic and igneous rocks. Crystals with less than 3–4 mol% substitution of Fe and Al for Ti have the space group $P2_1/a$ whereas those with more than 4 mol% (Al + Fe) have diffuse reflections $h + k$ = odd which become unobservable above 20 mol% substitution as the average structure approaches $A2/a$ symmetry (Higgins and Ribbe 1976; Oberti et al. 1991). The structural framework of titanite is formed by parallel chains of corner-sharing TiO_6 octahedra running along **a**. The parallel strings of octahedra are connected by GeO_4 tetrahedra sharing corners with the TiO_6 octahedra and by Ca in seven-coordination (Speer and Gibbs 1976; Taylor and Brown 1976).

At about $T_c = 487$ K, titanite undergoes a phase transition associated with a displacement of Ti atoms from the center of the TiO_6 octahedron (Ghose et al. 1991; Bismayer et al. 1992). Above the transition temperature the space group is $A2/a$ ($C2/c$) whereas below the space group is $P2_1/a$ ($P2_1/c$) (Taylor and Brown 1976; Ghose et al. 1991). The ordered low-temperature phase is characterized by alternating short and long Ti-O bonds along [100], with a reversed sense of Ti displacement in adjacent octahedral chains. In the $A2/a$-structure Ti is located at the centre of the TiO_6 octahedra. The transition is accompanied by the disappearance of superlattice diffraction maxima with $k + l = 2n + 1$. It is believed that the phase transition at 487 K involves merely a two-dimensional loss of long-range coherence between the off-center dipoles, while the structure remains ordered with respect to the (dynamic) Ti-displacement along individual octahedral chains (Malcherek et al. 2000). True $A2/a$ symmetry is thought to occur via a second, isosymmetric phase transition around $T_i = 825$ K. The first evidence for this second anomaly was obtained from excess birefringence (Bismayer et al. 1992) and Raman spectroscopy (Salje et al. 1993) measurements. Diffuse scattering intensity oriented in planes normal to [100] disappears close to T_i (Kek et al. 1997) and phonon bands associated with TiO_6 octahedral stretching modes exhibit strong softening at T_i (Zhang et al. 1997). Changes in the average crystal structure at T_i amount to small variations in the interatomic distances and angles (mainly reorientation of the Ca displacement vector and slight tilting of the TiO_6 octahedra; Zhang et al. 1997; Malcherek et al. 1999). The occurrence of non-classical effective critical exponents has been reported by a number of authors. Values of β have been given as 0.32 (Ghose et al. 1991) and close to 0.15 (e.g., Bismayer et al. 1992; Salje et al. 1993; Chrosch et al. 1997). More recently, Malcherek et al. (2000) and Hayward et al. (2000) both described the phase transition as tricritical, implying a classical value $\beta = 0.25$. Van Heurck et al. (1991) observed antiphase domains in the low temperature phase, with broad and mobile interfaces at and above T_c. When the temperature is further increased these antiphase domains disappear. Groat et al. (1996) found that similar behavior does not occur in malayaite, $CaSnOSiO_4$. Most probably, the transition in malayaite is similar to the isosymmetric transition at T_i in titanite. Robbins (1968) was the first to synthesize $CaTiOGeO_4$. X-ray precession photographs were indexed in $P2_1/n$ with $a = 6.65$, $b = 8.92$, and $c = 7.49$ Å, and $\beta = 119.45$. The present study reports displacive phase transitions in $CaTiOGeO_4$ and the solid solution it forms with titanite.

* E-mail: tmalch@min.uni-heidelberg.de

0003-004X/05/0809–1325$05.00/DOI: 10.2138/am.2005.1729

EXPERIMENTAL METHODS

Synthesis

Single crystals of $CaTiOGeO_4$ were synthesized from the oxides following the method described by Robbins (1968). CO_2 was driven off at 1323 K from a mixture of bulk composition $CaCO_3$·TiO_2·GeO_2 prior to melting in a welded platinum tube at 1723 K. Crystals were obtained by slowly cooling the stoichiometric melt at 3 K/h. The crystals were then held at 1273 K for 1 h and allowed to cool to room temperature. Colorless and transparent crystals were obtained. Wavelength-dispersive electron-microprobe analysis confirmed the stoichiometry. No impurities were observed in backscattered electron images.

Seven different samples at 5–20 mol% intervals across the solid solution $CaTiO(Ge_xSi_{1-x})O_4$ (CTGO*x*) were synthesized by solid-state reaction. The stoichiometric starting mixtures were prepared from pure fine-grained powders of $CaCO_3$ (Aldrich 20,293-2), TiO_2 (rutile, Aldrich 20,475-7), SiO_2 (Aldrich 38,126-8), and GeO_2 (Aldrich 19,947-8) at a maximum temperature of 1323 K. Approximately 2.5 g starting oxides were ground, pressed into pellets, and heated for several intervals of 5 days with intermittent grindings. Phase purity was established by powder diffraction analysis. Minor amounts of $CaTiO_3$ (~0.5 wt%) and $CaSiO_3$ (~1.5 wt%) were observed in samples CTGO10, CTGO70, and CTGO90.

Single-crystal X-ray diffraction

Single-crystal X-ray diffraction (XRD) data were collected at 293 K using an Enraf-Nonius CAD-4 automated four-circle diffractometer. A suitable crystal of $CaTiOGeO_4$ was selected and the quality checked using X-ray precession photographs. The crystal was bounded by the forms {001}, {$1\bar{1}0$}, and {$24\bar{1}$}. A numerical absorption correction based on the observed crystal shape was applied to the data using the program X-RED (STOE and Cie GmbH 1996). Intensity data were collected in the ω-2θ scan mode. The structure was refined using SHELX97 (Sheldrick 1997). Crystal data and parameters of the data collections are listed in Table 1.

X-ray powder diffraction

In situ X-ray powder diffraction measurements up to 1123 K were done using an Anton Paar HTK 1200 furnace mounted on a Philips Xpert diffractometer with monochromatic Cu$K\alpha_1$ radiation. Diffraction patterns were recorded in the range 17–90° 2θ using a proportional counter with 4 s/step counting time and a step size of 0.02°. Lattice parameters were determined using the LeBail method as implemented in the GSAS program (Larson and Von Dreele 1994) and the materials were refined with space group $A2/a$. The additional reflections with $k + l = 2n + 1$ that occur in the $P2_1/a$ phase are weak and mostly overlap the fundamental reflections. Additional Rietveld refinements were done at room temperature for all compounds across the solid solution. Starting fractional coordinates were taken from Ghose et al. (1991).

For CTGO50 and the end-member CTGO, the measurements were done up to 1073 and 1123 K, respectively. For the remaining compositions, measurements were done up to 773 K. In order to take into account the structural anomaly at T_i, the linear reference functions of thermal expansion were obtained using the high-temperature data above T_i from CTGO50 and the end-member compositions CTGO and titanite (latter data from Malcherek 2001). The slopes derived from extrapolation of the lattice constants were plotted against composition and fitted using a parabola. For the *c* lattice constant a straight-line fit was sufficient. With these fixed line slopes, individual linear functions of thermal expansion were obtained from the data measured up to 773 K for the remaining compositions.

TEM

$CaTiOGeO_4$ samples for transmission electron microscopy were prepared by adding copper grids to 10–15 µm thin samples. These specimens were ion milled and carbon coated. A double-tilt heating-holder was used for the in situ electron-diffraction experiments in a 300 kV Jeol JEM-3010 electron microscope. Electron-diffraction patterns were obtained along a number of zones at microscope temperature as well as in the vicinity of the transition. The disappearance or strong streaking of the $k + l$ = odd reflections was used as an indication that the transition temperature had been reached. The sample was stable under the electron beam at all temperatures.

TABLE 1. $CaTiOGeO_4$: Single crystal experimental data

Crystal data	
Radiation type	Mo$K\alpha$
Z	4
Temperature (K)	293 K
Space group	$P2_1/a$
a, *b*, *c* (Å)	7.158(1), 8.885(1), 6.649(1)
β (°)	113.834(1)
V (Å^3)	386.84(9)
Size (mm)	0.3 × 0.2 × 0.15
No. of reflections for cell parameters	24
Data collection	
Diffractometer	Enraf-Nonius CAD-4
Data collection method	ω-2θ
θ_{max} (°)	35
Range of *h*, *k*, *l*	$\bar{1}1 - 10$, $\bar{1}4 - 14$, 0 – 10
No. of standard reflections	3
No. of measured, independent and observed reflections	3648, 1704, 1470
R_{int}	0.0214
Absorption correction	Numerical
Refinement	
Refinement	Full-matrix least squares on F^2
Weighing scheme	$w = 1/[\sigma^2(F_o^2) + (WP)^2 + 0.01P]$ where $P = (F_o^2 + 2F_c^2)/3$
W	0.0378
$R[F^2 > 2\sigma(F^2)]$, $wR(F^2)$, *S*(GooF)	0.0252, 0.0637, 1.131
No. of reflections, restraints and parameters used in refinement	1704, 0, 74
Extinction coefficient	0.0018(5)

RESULTS

Structure of $CaTiOGeO_4$

Robbins (1968) first synthesized $CaTiOGeO_4$ and discussed its structure on the basis of X-ray precession films, which showed $P2_1/n$ symmetry using the setting of Zachariasen (1930) and suggested a structure similar to that of titanite. In order to compare the results of Robbins (1968) with our own it was necessary to transform the $P2_1/n$ setting to the $P2_1/a$ setting. Applying the transformation matrix (101,010,$\bar{1}$00) to the lattice constants derived by Robbins (1968) gave: $a = 7.13$, $b = 8.92$, and $c = 6.65$ Å, and $\beta = 114.28°$. Considering the esd of the lattice parameters given by Robbins (1968), this agrees with our results. The lattice parameters are also consistent with the data given in PDF entry no. 40-387. The structure of CTGO was refined in space group $P2_1/a$. CTGO is isostructural with titanite. Unit-cell data, atom coordinates, and interatomic distances for the single crystal structure refinement are given in Tables 1–3.

Structure refinement across $CaTiO(Ge_xSi_{1-x})O_4$

The refined structural parameters at room temperature are given in Table 4[1]. The variation of the mean bond lengths is displayed in Table 5. For comparison of the corresponding lengths and angles for titanite see Kek et al. (1997). The bond length of Ca-O is constant within the limits of the measurement accuracy, while as expected, the mean bond length of Ge to the

[1] Deposit item AM-05-021, Tables 4 and 8. Deposit items are available two ways: For a paper copy contact the Business Office of the Mineralogical Society of America (see inside front cover of recent issue) for price information. For an electronic copy visit the MSA web site at http://www.minsocam.org, go to the American Mineralogist Contents, find the table of contents for the specific volume/issue wanted, and then click on the deposit link there.

TABLE 2. $CaTiOGeO_4$: Atomic positional parameters and anisotropic thermal displacement parameters (Å²) at room temperature

	Ca	Ti	Ge	O1	O2A	O2B	O3A	O3B
x	0.2428(1)	0.5161(1)	0.7478(1)	0.7498(2)	0.9199(2)	0.0772(2)	0.3926(2)	0.6095(2)
y	0.4215(1)	0.2545(1)	0.4334(1)	0.3179(2)	0.3097(2)	0.1902(2)	0.4576(2)	0.0441(2)
z	0.2503(1)	0.7492(1)	0.2487(1)	0.7507(2)	0.4385(2)	0.0578(2)	0.6422(2)	0.8567(2)
U11	0.0158(2)	0.0047(1)	0.0049(9)	0.0051(4)	0.0103(4)	0.0094(4)	0.0085(4)	0.0084(4)
U22	0.0071(1)	0.0056(6)	0.0055(1)	0.0074(4)	0.0095(4)	0.0100(4)	0.0072(4)	0.0072(4)
U33	0.0066(2)	0.0041(1)	0.0039(1)	0.0096(5)	0.0057(4)	0.0056(4)	0.0082(4)	0.0078(4)
U23	0.00001(7)	−0.0002(7)	−0.00006(4)	−0.0001(3)	0.0018(3)	0.0021(3)	0.0007(3)	0.0006(3)
U13	0.0014(1)	0.0021(9)	0.0022(6)	0.0035(4)	0.0018(4)	0.0024(3)	0.0052(4)	0.0050(4)
U12	0.0005(1)	0.0002(6)	−0.00004(3)	−0.0005(2)	0.0029(3)	0.0028(3)	0.0023(3)	0.0021(3)

surrounding oxygen atoms increases with increasing Ge content. The composition dependence of the mean bond length of Ti is near symmetric with the end-members exhibiting the shortest average bond lengths.

TEM

Electron diffraction patterns were obtained for a number of zones at temperatures spanning the transition. The diffraction patterns show two families of spots (Fig. 1a): sharp and intense spots with $k + l$ = even and weak super-structure reflections with $k + l$ = odd. As the temperature increases, the diffuse scattering becomes visible and finally at $T > T_c$ degenerates to almost continuous streaks elongated along **b***. In analogy to titanite (Higgins and Ribbe 1976), the streaks would result from planes of diffusely scattered intensity perpendicular to the octahedral chains. The spots with $k + l$ = even remained round and sharp and their intensities showed no appreciable change on heating. Figure 1a-d shows the [001] zone below and above T_c.

In the low-temperature phase, antiphase boundaries can be observed using dark-field mode. A series of dark-field contrast images made with the (110) and $(2\bar{1}0)$ superstructure reflections is shown in Figures 2a–c. The geometrical features are consistent with the assumption that the antiphase domains have a cylindrical shape. Straight sections of the cylinder walls are oriented parallel to **a**, i.e., parallel to the chains of TiO_6 octahedra (Van Heurck et al. 1991). During heating to above T_c, the domains are not mobile, but disappear somewhat above the phase transition. On renewed cooling below T_c the interfaces reappear at the same location as during heating. This memory effect may be due to pinning of the domain walls by defects or by the specimen boundaries. This is not in agreement with the behavior observed in titanite. Van Heurck et al. (1991) found that the antiphase domains become mobile until they disappear somewhat above the phase transition. Higgins and Ribbe (1976) observed such antiphase domains in titanite at room temperature using the $k + l$ = odd reflections indicative of $P2_1/a$ symmetry. They concluded that the antiphase domains are linear and parallel to *a*. This behavior is in agreement with our observations for $CaTiOGeO_4$.

Lattice parameters

The $A2/a$-$P2_1/a$ structural phase transition in $CaTiOGeO_4$ was observed using in situ heating X-ray powder diffraction methods. Diffraction patterns were recorded in the temperature range 298–1123 K. On the basis of the disappearance of $k + l$ = odd reflections the transition can be observed in the diffraction patterns. At low temperatures these clearly exhibit the $k + l$ = odd reflections indicative of $P2_1/a$ symmetry. The intensities of the $22\bar{1}$ and $21\bar{2}$ superlattice reflections were extracted using the LeBail fit in space group $P2_1/a$. The superlattice reflections show a steady decrease with increasing temperature, but due to

TABLE 3. $CaTiOGeO_4$: interatomic distances (Å) and angles (°) at room temperature

Ti-O1	1.762(1)	O1-Ti-O2A	91.56(5)
Ti-O1′	2.016(1)	O1-Ti-O2B	95.95(5)
Ti-O2A	1.980(1)	O1-Ti-O3A	89.76(5)
Ti-O2B	1.979(1)	O1-Ti-O3B	96.68(5)
Ti-O3A	2.009(1)	O1′-Ti-O2A	88.97(4)
Ti-O3B	2.017(1)	O1′-Ti-O2B	83.53(4)
		O1′-Ti-O3A	90.38(5)
Mean	1.960	O1′-Ti-O3B	83.18(5)
		O2A-Ti-O3A	88.97(4)
Ca-O1	2.316(1)	O2A-Ti-O3B	91.63(4)
Ca-O2A	2.473(1)	O2B-Ti-O3A	91.45(5)
Ca-O2B	2.459(1)	O2B-Ti-O3B	87.71(5)
Ca-O3A	2.405(1)		
Ca-O3B	2.415(1)	Ti-O1-Ti	142.74(7)
Ca-O3A′	2.639(1)		
Ca-O3B′	2.570(1)	O2A-Ge-O2B	102.18(6)
		O2A-Ge-O3A	113.82(5)
Mean	2.468	O2A-Ge-O3B	106.66(5)
		O2B-Ge-O3A	107.37(5)
Ge-O2A	1.749(1)	O2B-Ge-O3B	114.23(5)
Ge-O2B	1.748(1)	O3A-Ge-O3B	112.30(6)
Ge-O3A	1.750(1)		
Ge-O3B	1.755(1)		
Mean	1.751		

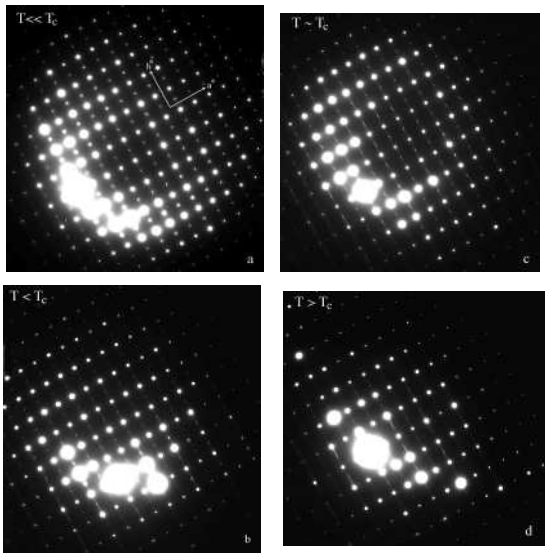

FIGURE 1. Evolution of the electron diffraction patterns with temperature for the [001] zone. With increasing temperature the streaking along **b*** increases in the zone. At $T > T_c$ the spots with $k + l$ = odd are gone.

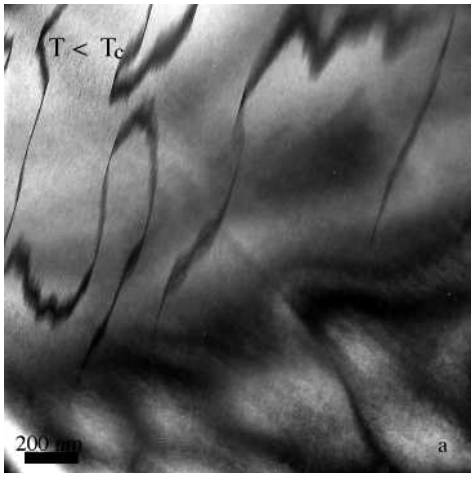

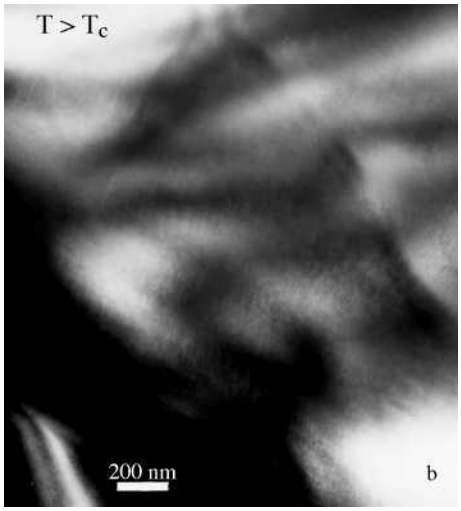

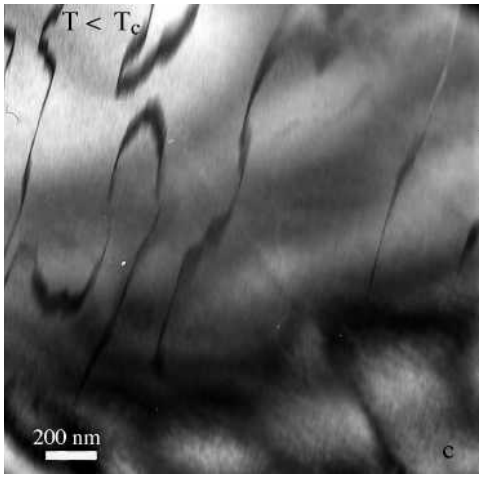

FIGURE 2. Diffraction contrast images of domain boundaries as a function of temperature. The domain boundaries disappear at some temperature above T_c but appear at the same place when the temperature is decreased.

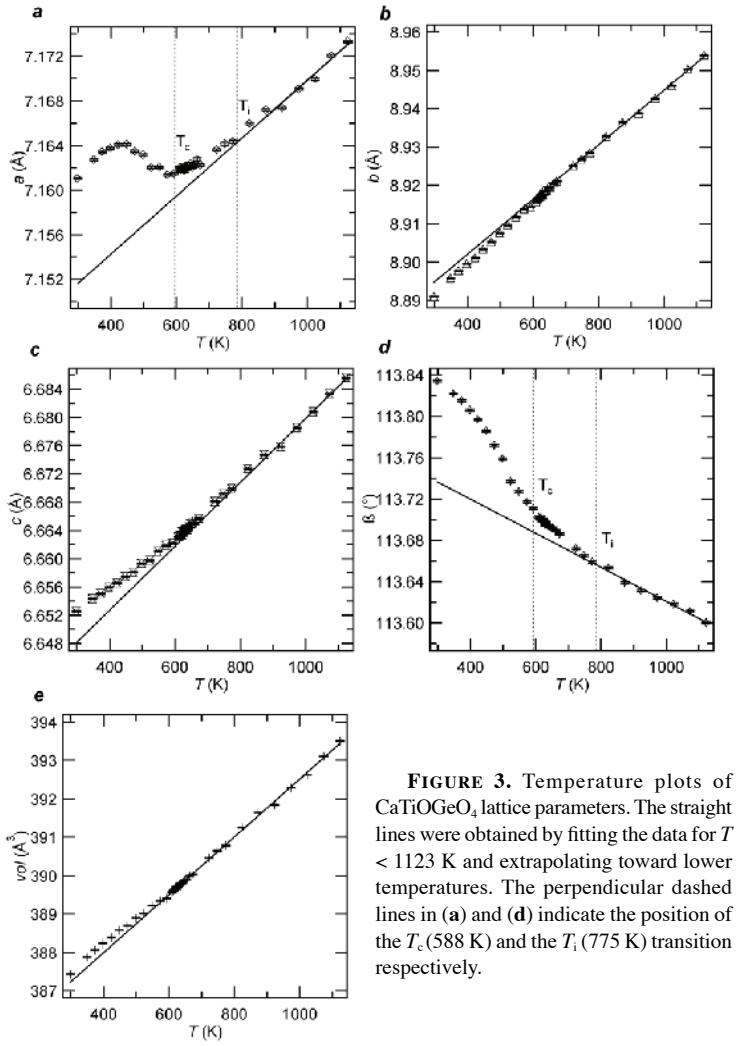

FIGURE 3. Temperature plots of $CaTiOGeO_4$ lattice parameters. The straight lines were obtained by fitting the data for T < 1123 K and extrapolating toward lower temperatures. The perpendicular dashed lines in (**a**) and (**d**) indicate the position of the T_c (588 K) and the T_i (775 K) transition respectively.

background noise and their relatively small intensity it is not possible to determine the exact critical temperature in this way. Within the temperature range 523 to 623 K the $P2_1/a$ reflections disappear, but below this temperature range they are clearly visible. By extrapolation of the lattice parameters measured for T < 1123 K toward lower temperatures, linear reference functions of thermal expansion were obtained for all lattice parameters. The complete set of lattice parameter data for CTGO is shown in Figure 3a–e. The transition is accompanied by a significant expansion of **a**. Another significant deviation from the extrapolated high temperature data is seen for the monoclinic angle β. In the case of *b* only minor deviation from linear thermal expansion occurs over the entire temperature range. Likewise, only very small positive deviation occurs for the *c* lattice dimension. From the *a* lattice constant and the β angle, there are clear indications in analogy to titanite for the additional occurrence of an isosymmetric anomaly at T_i in $CaTiOGeO_4$ (Figs. 3a and d). T_i for CTGO can be estimated as 800 ± 25 K, in accordance with the estimates for T_i in titanite (Malcherek 2001; Kek et al. 1997; Zhang et al. 1997). Measurement temperatures and lattice parameters are given in Table 6.

Titanite and CTGO form a complete solid solution, with no

TABLE 5. Mean bond lengths (Å) at room temperature using S.G. $P2_1/a$

Mol% Ge	Ge-O	Ti-O	Ca-O
CTGO	1.752	1.964	2.468
95	1.768	1.972	2.432
90	1.776	1.975	2.443
70	1.718	1.981	2.436
50	1.710	1.973	2.436
30	1.652	1.978	2.469
20	1.620	1.965	2.487
10	1.643	1.975	2.453
CTSO	1.651	1.957	2.432

Notes: Bond lengths for titanite taken from Kek et al. (1997).

TABLE 6. $CaTiOGeO_4$: Lattice parameters as a function of the temperature

T (K)	a (Å)	b (Å)	c (Å)	β (°)
298	7.16144(6)	8.89229(2)	6.65311(4)	113.833(1)
348	7.16210(5)	8.89500(8)	6.65392(5)	113.828(1)
373	7.16264(7)	8.89658(6)	6.65428(6)	113.813(1)
398	7.16369(8)	8.89933(6)	6.65583(6)	113.806(1)
423	7.16373(6)	8.90061(7)	6.65640(8)	113.797(1)
448	7.16389(4)	8.90310(8)	6.65731(7)	113.787(1)
473	7.16336(7)	8.90510(5)	6.65812(8)	113.773(1)
498	7.16288(7)	8.90736(5)	6.65924(7)	113.758(1)
523	7.16210(6)	8.90963(6)	6.65999(5)	113.741(1)
548	7.16187(8)	8.91164(6)	6.66099(5)	113.729(1)
573	7.16135(5)	8.91345(7)	6.66185(8)	113.719(1)
593	7.16147(6)	8.91441(4)	6.66218(8)	113.711(1)
610	7.16198(6)	8.91560(6)	6.66303(7)	113.702(1)
613	7.16181(8)	8.91642(4)	6.66322(7)	113.701(1)
615	7.16197(7)	8.91662(5)	6.66319(5)	113.702(1)
618	7.16193(6)	8.91687(7)	6.66333(4)	113.699(1)
621	7.16194(7)	8.91732(9)	6.66382(6)	113.699(1)
623	7.16170(9)	8.91699(8)	6.66334(6)	113.700(2)
625	7.16202(6)	8.91760(7)	6.66384(6)	113.699(1)
628	7.16212(6)	8.91734(7)	6.66371(9)	113.695(1)
630	7.16209(8)	8.91754(8)	6.66398(6)	113.696(1)
633	7.16195(6)	8.91866(6)	6.66411(5)	113.697(1)
638	7.16211(7)	8.91843(6)	6.66405(8)	113.694(1)
643	7.16235(5)	8.91862(8)	6.66446(8)	113.693(2)
648	7.16201(5)	8.91959(9)	6.66490(7)	113.692(1)
653	7.16217(6)	8.91935(8)	6.66499(6)	113.692(1)
663	7.16273(6)	8.92046(7)	6.66530(6)	113.689(1)
673	7.16223(8)	8.92107(6)	6.66567(8)	113.686(1)
723	7.16361(7)	8.92515(6)	6.66807(7)	113.672(2)
748	7.16414(9)	8.92676(5)	6.66918(7)	113.665(1)
773	7.16433(6)	8.92847(7)	6.66989(6)	113.659(2)
823	7.16597(7)	8.93272(8)	6.67272(8)	113.653(1)
873	7.16718(7)	8.93646(7)	6.67470(4)	113.639(1)
923	7.16736(6)	8.93874(8)	6.67581(4)	113.631(1)
973	7.16906(8)	8.94262(9)	6.67852(5)	113.624(1)
1023	7.16993(8)	8.94597(7)	6.68077(6)	113.618(1)
1073	7.17204(7)	8.95028(5)	6.68332(7)	113.611(1)
1123	7.17332(8)	8.95395(6)	6.68559(6)	113.600(2)

TABLE 7. Lattice parameters for $CaTi(Ge_xSi_{1-x})O_4$ at room temperature

Mol% Ge	a (Å)	b (Å)	c (Å)	β (°)	V (Å^3)
100	7.16144(6)	8.89229(2)	6.65311(4)	113.833(1)	387.552(5)
95	7.14287(6)	8.87820(6)	6.64268(3)	113.776(1)	385.500(2)
90	7.13460(4)	8.87346(4)	6.63886(9)	113.738(1)	384.738(7)
70	7.11815(6)	8.83215(7)	6.61777(5)	113.767(1)	380.765(6)
50	7.09534(4)	8.79173(3)	6.59620(8)	113.757(1)	376.606(6)
30	7.09137(7)	8.78567(7)	6.59344(5)	113.766(1)	375.952(6)
20	7.07182(5)	8.74371(5)	6.57304(7)	113.782(1)	371.925(4)
10	7.06582(8)	8.73056(7)	6.56626(5)	113.782(1)	370.668(5)

evidence for phase separation at any of the intermediate compositions. Lattice constants derived from Rietveld refinements for all intermediate compositions at room temperature are given in Table 7 and are displayed in Figure 4. Across the solid solution, replacement of Si by Ge leads to a gradual increase in cell volume by 4.5%. The a, b, and c lattice parameters increase across the solid solution, while β shows a non-linear behavior as the Ge content increases. The end-member compositions have a larger β angle than the intermediate compositions. The complete set of lattice parameter data is given in Table 8[2]. Lattice parameters for each of the compositions, extracted from the LeBail analysis, show a very similar evolution with temperature as for CTGO and titanite.

Spontaneous strain in $CaTiOGeO_4$

One of the most significant physical effects that accompany a structural phase transition is lattice strain. Strain components were calculated according to the equations given by Carpenter et al. (1998). The scalar spontaneous strain is defined as

$$e_s = (\Sigma e_{ij}^2)^{1/2}$$

In the case of a zone-boundary transition, this property is proportional to the square of the order parameter Q of the transition. The spontaneous strain associated with the $P2_1/a$-$A2/a$ phase transition in CTGO is relatively small (Fig. 5). By linear extrapolation of e_s^2 to zero, the transition temperature is estimated as $T_c = 588 \pm 4$ K, which coincides with the onset of volume strain (Fig. 3e). In agreement with previous work on synthetic titanite (Malcherek 2001), the spontaneous strain due to the $P2_1/a$-$A2/a$ phase transition in $CaTiOGeO_4$ is dominated by the components e_{11} and e_{13}. The e_{22} and e_{33} components are nearly equal in magnitude and both are small and negative for $T < T_c$, e_{22} being the more negative. The e_{22} component differs from that in titanite, as its contribution to the strain cannot be completely neglected. The component e_{11} does not disappear at T_c but remains finite up to T_i (Fig. 5) in CTGO. The scalar strain (Fig. 6) has been determined and the strain for titanite (Malcherek 2001) is plotted for comparison. The square of the scalar strain (Fig. 7) is approximately linear with temperature above 400 K, which, as $e^2 \sim Q^4$, implies that the transition is close to tricritical.

Spontaneous strain in the solid-solution $CaTiO(Ge_xSi_{1-x})O_4$

The strain components (Figs. 8a–d) show a continuous, but non-linear, evolution from room-temperature values to 773 and 1073 K for CTGO50 and 1123 K for CTGO. The component e_{22} (Fig. 8c) is in most cases very close to zero within the limits of accuracy. The component e_{33} is negative but near zero for $T < T_c$. The e_{11} component is positive below T_c whereas the e_{13} component is negative. The strain components show a similar evolution for all intermediate compositions across the solid solution, with the exception of e_{22}. A small volume strain is observed.

The magnitude of the strain component e_{11} decreases from titanite (data from Malcherek 2001) to CTGO (Fig. 8a). In contrast, the e_{13} component shows a nearly symmetric variation, with the

[2] Deposit item AM-05-021, Tables 4 and 8. Deposit items are available two ways: For a paper copy contact the Business Office of the Mineralogical Society of America (see inside front cover of recent issue) for price information. For an electronic copy visit the MSA web site at http://www.minsocam.org, go to the American Mineralogist Contents, find the table of contents for the specific volume/issue wanted, and then click on the deposit link there.

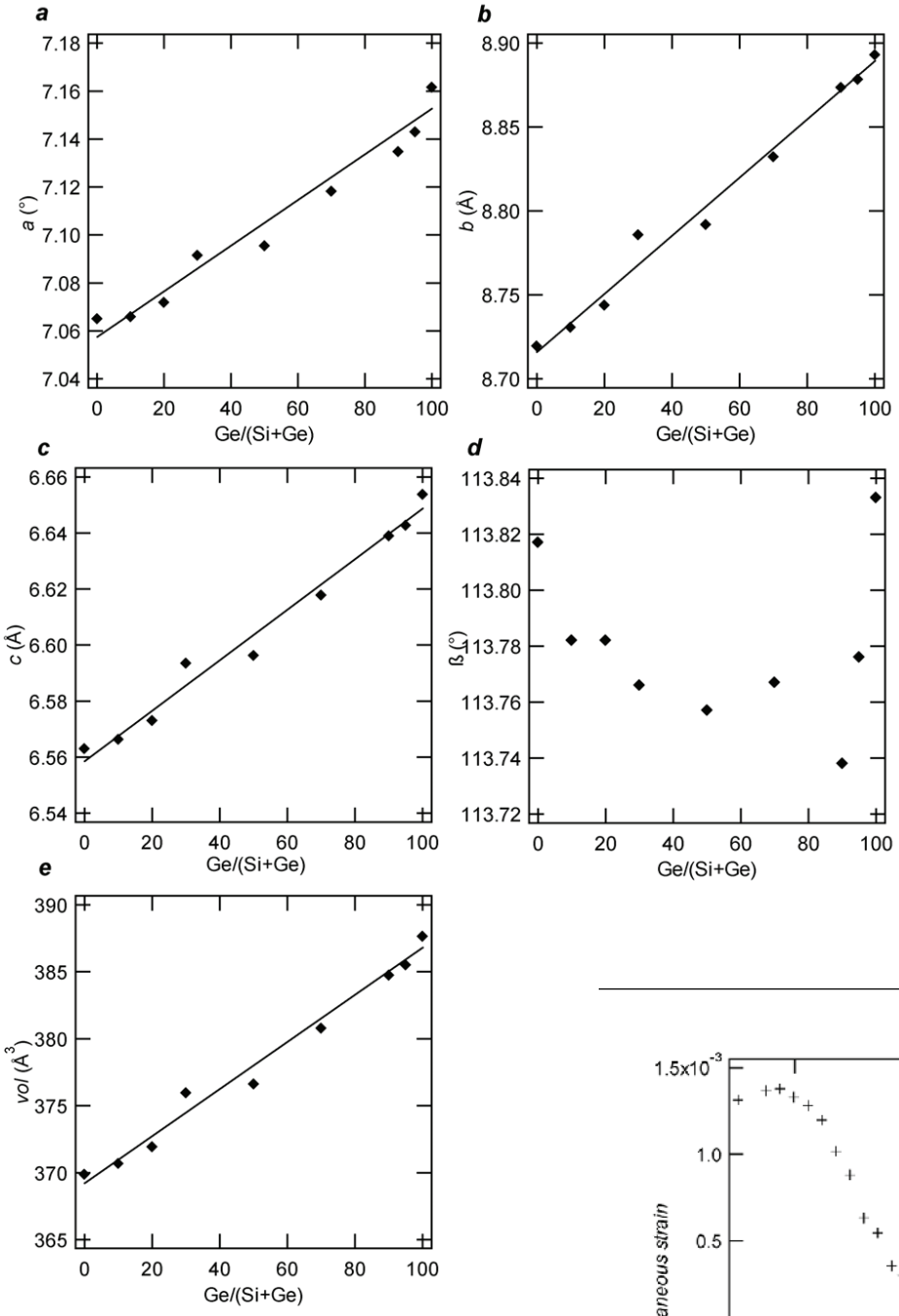

FIGURE 4. The solid solution $CaTiO(Ge_xSi_{1-x})O_4$. Lattice constants as a function of Ge content at room temperature.

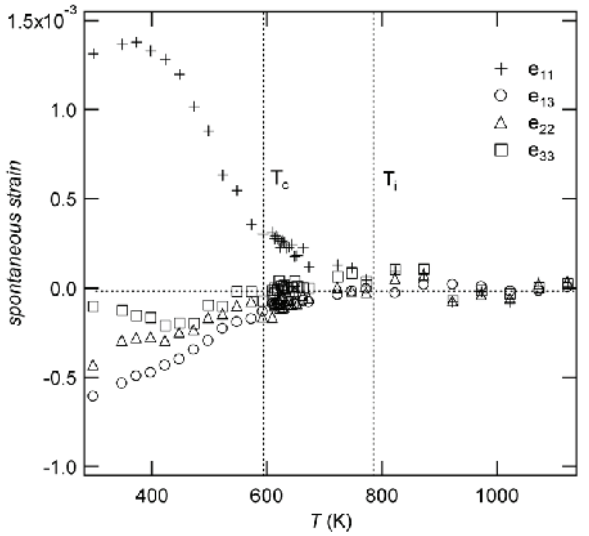

FIGURE 5. Strain components for $CaTiOGeO_4$ as a function of temperature. Only the components e_{11} and e_{13} contribute significantly to the strain.

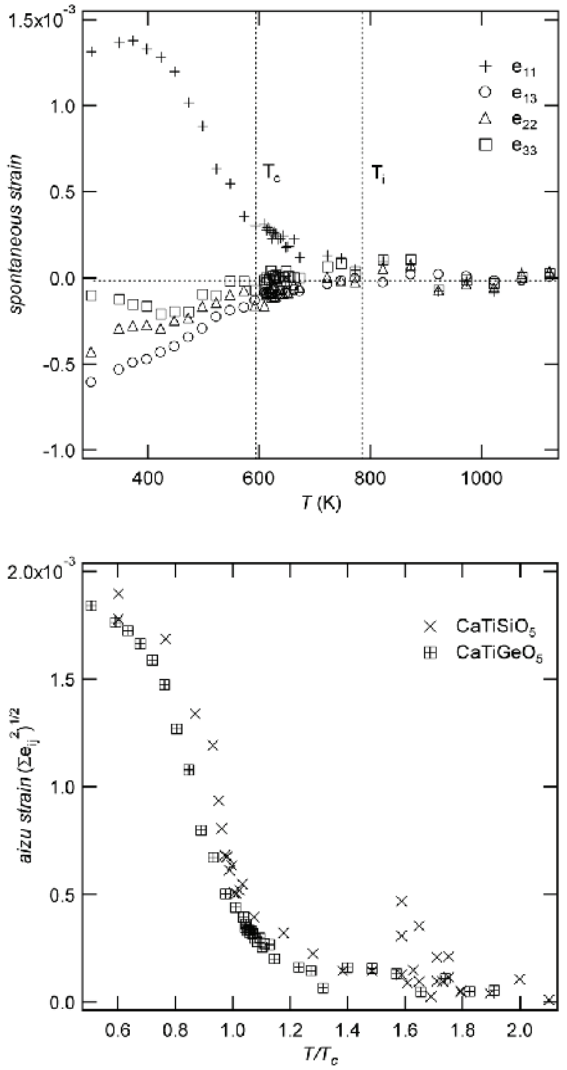

FIGURE 6. The scalar strain (aizu strain) for $CaTiOGeO_4$ and titanite (data from Malcherek 2001) as a function of temperature.

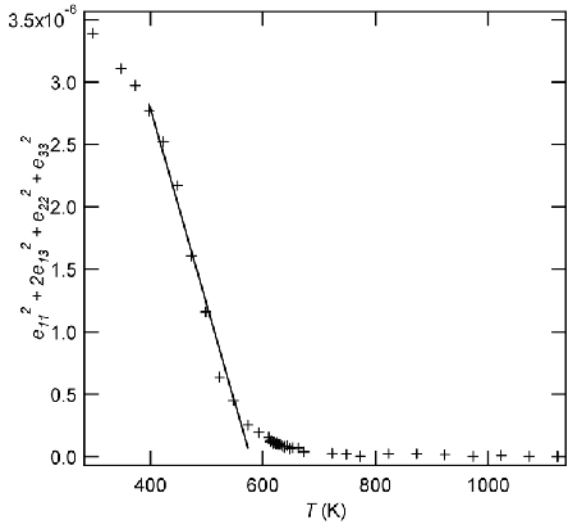

FIGURE 7. The square of the scalar strain for $CaTiOGeO_4$. The linearity at $T < T_c = 588$ K indicates the tricritical behavior.

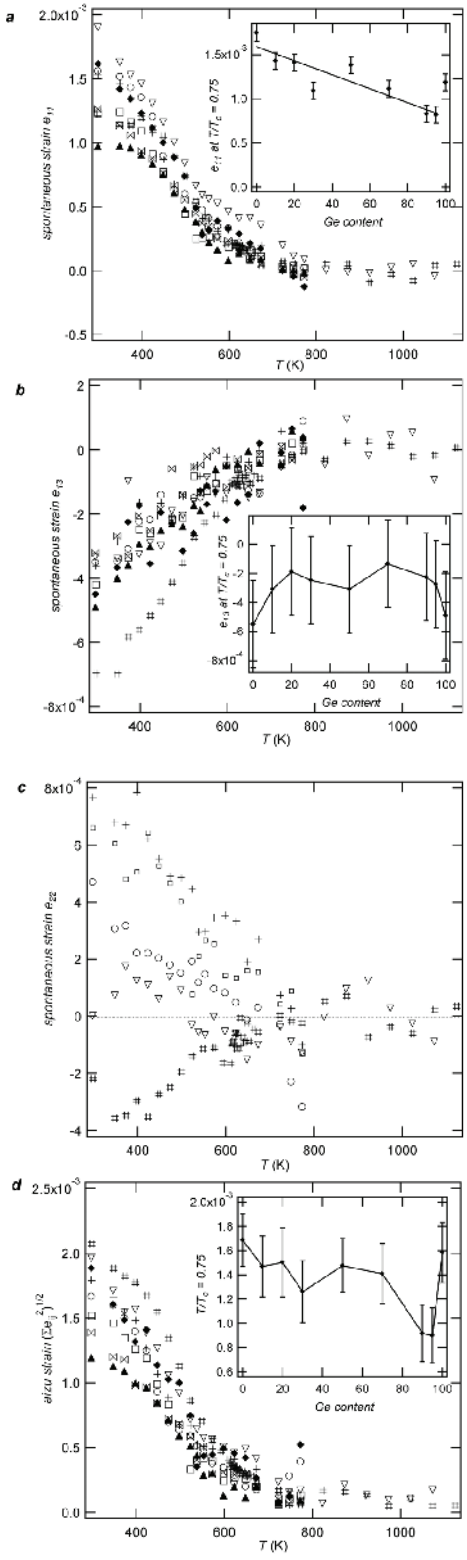

FIGURE 8. Strain components e_{11} (**a**), e_{13} (**b**), e_{22} (**c**), and the scalar strain (**d**) for all intermediate compounds as a function of temperature. The insets show the strain component at the reduced temperature $T/T_c = 0.75$ as a function of Ge content.

end-members having the most pronounced negative values and with intermediate compositions showing less shear strain (Fig. 8b). Overall, the scalar strain is constant across the solid solution (Fig. 8d). The compositions CTGO90 and CTGO95 deviate most by having a slightly smaller scalar strain, 0.0014 and 0.0011, respectively, compared to 0.0016 in $CaTiOGeO_4$.

From the e_{11} strain component of CTGO50 and CTGO (Fig. 8a) it is evident that the isosymmetric phase transition observed in titanite occurs across the entire solid solution. This has a significant influence on the evolution of e_{11} as it is finite at temperatures above T_c and vanishes only at $T_i \approx 800$ K.

The square of the scalar strain, Σe_{ij}^2, for the intermediate compositions (Fig. 9a–g) shows linear dependence on temperature over a wide range below the respective transition temperatures, T_c. Again this does hint toward tricritical character of the transition, just as in the end-members. Based on the strain analysis, T_c for all compositions along the solid solution was determined by extrapolation of e_s^2 to zero. T_c increases almost linearly from 487 K in titanite to 588 K in CTGO (Fig. 10). Determination of the isosymmetric transition temperature T_i is encumbered by large errors because of the way the extrapolation was done, but it appears to remain more or less constant at 800 ± 25 K.

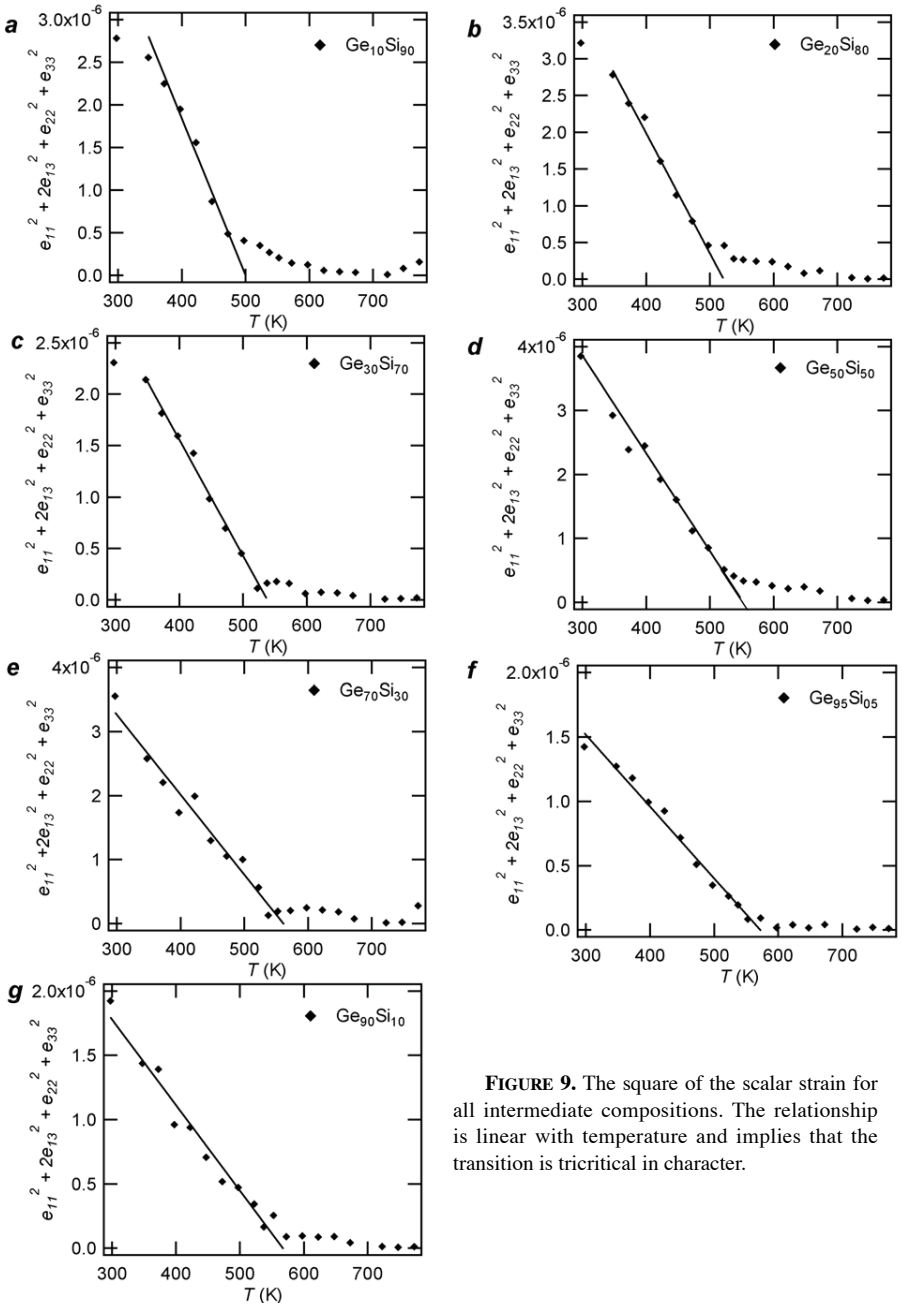

FIGURE 9. The square of the scalar strain for all intermediate compositions. The relationship is linear with temperature and implies that the transition is tricritical in character.

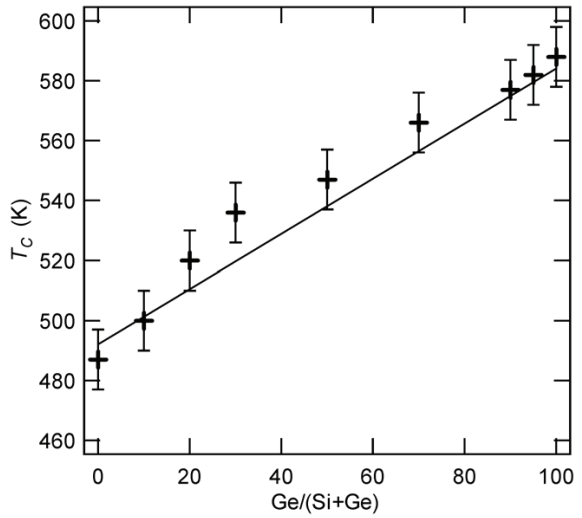

FIGURE 10. Transition temperature, T_c across the solid solution, $CaTiO(Ge_xSi_{1-x})O_4$. T_c = 588 K for $CaTiOGeO_4$ and 487 K for titanite.

DISCUSSION

From Figure 10 it is clear that the substitution of Ge for Si has a marked influence on T_c. The evolution of T_c with composition is nearly linear and is marked by a gradual increase of nearly 100 K from the titanite end-member toward CTGO. Thus the substitution of Ge for Si stabilizes the ordered $P2_1/a$ phase. On the other hand, the isostructural anomaly T_i appears to be constant at 800 K. Zhang et al. (1997) conclude that the high-temperature phase transition in titanite shows a completely different behavior than the transition at T_c = 487 K. They observed that Fe and Al substituting for Ti have much less effect on the transition near 825 K than on that at 487 K, where substitution at the octahedral site has a large effect and the transition is eventually suppressed. The effect of Fe, Al substitution in titanite is to block the lower-temperature transition, whereas substitution of Ge for Si has the opposite effect. On the other hand, T_i is neither sensitive to substitution at the octahedral site, nor do our results suggest that it is significantly altered by substitutions at the tetrahedral site.

The e_{13} component is close to zero for most of the intermediate compositions (Fig. 8b). This implies that the shearing of the unit cell is lessened for intermediate compositions. At the same time, the magnitude of e_{11} decreases with increasing T_c and Ge content. A possible explanation might involve the introduction of a minor strain along **b** as suggested by the e_{22} component. As the scalar strain is near constant across the solid solution, the decreasing strain due to expansion along **a** has to be compensated. A significant difference in strain behavior between titanite (Malcherek 2001) and CTGO is the presence of a minor negative strain along **b** expressed by the strain component e_{22} with a minimum of –0.00036. A similar trend is observed in CTGO20, CTGO30, and CTGO70 but with opposite sign.

The component e_{11} for the end-member composition $CaTiOGeO_4$ does not disappear at T_c but remains finite up to T_i (Fig. 5b). This behavior is different from that observed in titanite. In titanite, it is only the e_{13} component that is finite above T_c and it vanishes at T_i (Malcherek 2001).

The composition dependence of the mean Ti-O bond length does not correlate with the transition temperature, T_c, i.e., the bond length does not increase with increasing T_c (Table 5 and Fig. 11). Instead it shows a similar evolution as the strain component e_{13} (Fig. 12). There is correlation between the shear strain and the Ti-O mean bond length (Fig. 12). Hammonds et al. (1998) predicted that due to the absence of rigid unit modes in the titanite structure, polyhedral distortion is to be expected upon chemical substitution in titanite, rather than polyhedral tilting. Variation of the individual bond lengths is more pronounced for the intermediate compounds than for the end-member compositions and as a result the octahedra and tetrahedra are more distorted. Kunz et al. (1997) observed increasing Ca-O bond lengths with increasing Sn content at the octahedral site of the titanite-malayaite join. In our case, near constant Ca-O bond lengths are observed with increasing substitution by Ge for Si at the tetrahedral site.

A comparison of the single crystal data for $CaTiOGeO_4$ with the data for titanite (Kek et al. 1997) shows that the most significant difference between the two isomorphs is the bond

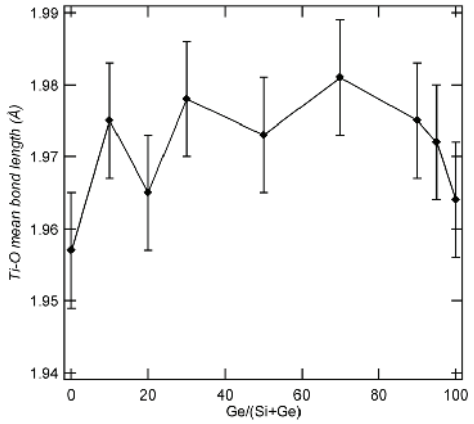

FIGURE 11. The mean bond length Ti-O as a function of Ge content.

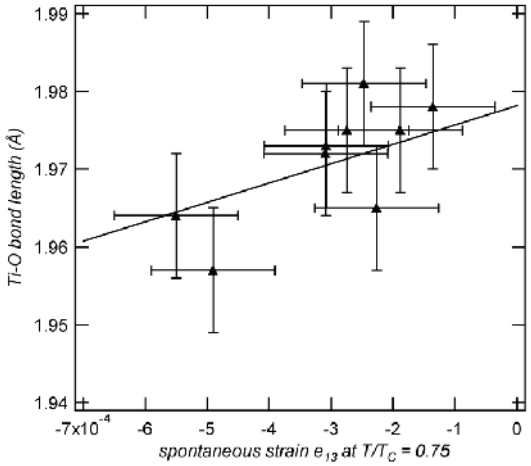

FIGURE 12. Correlation between Ti-O and the shear strain e_{13}.

lengths Ti-O1 and Ti-O1'. For $CaTiOGeO_4$ these are 1.7615 and 2.0165 Å, respectively (Δ = 0.255 Å). For titanite they are Ti-O1 = 1.754 Å and Ti-O1' = 1.989 Å (Δ = 0.235 Å). The larger Ti displacement in CTGO compared to titanite is in accordance with the higher transition temperature observed in CTGO, if one assumes an Abrahams-Kurtz-Jamieson relation between T_c and cation displacement (Abrahams et al. 1968). Tilting of the TiO_6 octahedra is slightly smaller in CTGO, with a Ti-O1-Ti angle of ~143° compared to 141° in titanite (Ghose et al. 1991). This straightening of the octahedral chains can be attributed to the larger size of the GeO_4 tetrahedra. The bond valence sum (BVS, calculated according to Brese and O'Keefe 1991) for the Ge site in CTGO has an almost ideal value of 3.97, while the BVS for Si in titanite is less than ideal (3.73), hinting at tensile stress in the Si-coordination of titanite. As in titanite, Ti is slightly overbonded in CTGO, with a constant BVS close to 4.2 across the entire solid solution. However, distortion of the TiO_6 octahedron is less in CTGO.

ACKNOWLEDGMENTS

Financial support through the Deutsche Forschungs-Gemeinschaft (DFG) is gratefully acknowledged.

REFERENCES CITED

Abrahams, S.C., Kurtz, S.K., and Jamieson, P.B. (1968) Atomic displacement relationship to Curie temperature and spontaneous polarization in displacive ferroelectrics. Physical Review, 172, 551–553.

Bismayer, U., Schmahl, W., Schmidt, C., and Groat, L.A. (1992) Linear birefringence and X-ray diffraction studies of the structural phase transition in titanite, $CaTiSiO_5$. Physics and Chemistry of Minerals, 19, 260–266.

Brese, N.E. and O'Keeffe, M. (1991) Bond-valence parameters for solids. Acta Crystallographica, B47, 192–197.

Carpenter, M.A., Salje, E.K.H., and Graeme-Barber, A. (1998) Spontaneous strain as a determinant of thermodynamic properties for phase transitions in minerals. European Journal of Mineralogy, 10, 621–691.

Chrosch, J., Bismayer, U., and Salje, E.K.H. (1997) Anti-phase boundaries and phase transitions in titanite: An X-ray diffraction study. American Mineralogist, 82, 677–681.

Ghose, S., Ito, Y., and Hatch, D.M. (1991) Paraelectric-antiferroelectric phase transition in titanite, $CaTiSiO_5$: I. A high temperature X-ray diffraction study of the order parameter and transition mechanism. Physics and Chemistry of Minerals, 17, 591–603.

Groat, L.A., Kek, S., Bismayer, U., Schmidt, C., Krane, H.G., Meyer, H., Nistor, L., and Van Trendeloo, G. (1996) A synchrotron radiation, HRTEM, X-ray powder diffraction, and Raman spectroscopy study of malayaite, $CaSnSiO_5$. American Mineralogist, 81, 595–602.

Hammonds, K.D., Bosenik, A., Dove, M.T., and Heine, V. (1998) Rigid unit modes in crystal structures with octahedrally coordinated atoms. American Mineralogist, 83, 476–497.

Hawthorne, F.C., Groat, L.A., Raudsepp, M., Ball, N.A., Kimata, M., Spike, F.D., Gaba, R., Halden, N.M., Lumpkin, G.R., Ewing, R.C., Gregor, R.B., Lytle, F.W., Ercit, T.S., Rossman, G.R., Wicks, F.J., Ramik, R.A., Sherriff, B.L., Fleet, M.E., and McCammon, C. (1991) Alpha-decay damage in titanite. American Mineralogist, 76, 370–396.

Hayward, S.A., del Cerro, J., and Salje, E.K.H. (2000) Antiferroelectric phase transition in titanite: Excess entropy and short range order. American Mineralogist, 85, 557–562.

Higgins, J.B. and Ribbe, P.H. (1976) The crystal chemistry and space groups of natural and synthetic titanites. American Mineralogist, 61, 878–888.

Kek, S., Aroyo, M., Bismayer, U., Schmidt, C., Eichhorn, K., and Krane, H.G. (1997). The two-step phase transition of titanite, $CaTiSiO_5$: a synchrotron radiation study. Zeitschrift für Kristallographie, 212, 9–19.

Kunz, M., Xirouchakis, D., Wang, Y., Parise, J.B., and Lindsley, D.H. (1997) Structural investigations along the join $CaTiOSiO_4$-$CaSnOSiO_4$. Schweizerische Mineralogische und Petrographische Mitteilungen, 77, 1–11.

Kunz, M., Arlt, T., and Stolz, J. (2000) In situ powder diffraction study of titanite ($CaTiOSiO_4$) at high pressure and high temperature. American Mineralogist, 85, 1465–1473.

Larson, A.C. and Von Dreele, R.B. (1994) General Structure Analysis System (GSAS). Los Almos National Laboratory. Los Alamos, New Mexico.

Malcherek, T. (2001) Spontaneous strain in synthetic titanite, $CaTiOSiO_4$. Mineralogical Magazine, 65, 709–715.

Malcherek, T., Domeneghetti, C.M., Tazzoli, V., Salje, E.K.H., and Bismayer, U. (1999) A high temperature study of synthetic titanite $CaTiOSiO_4$. Phase Transitions, 69, 119–131.

Malcherek, T., Paulmann, C., Domeneghetti, M.C., and Bismayer, U. (2000) Diffuse scattering anisostropy and the $P2_1/a \leftrightarrow A2/a$ phase transition in titanite, $CaTiOSiO_4$. Journal of Applied Crystallography, 34, 108–113.

Oberti, R., Smith, D.C., Rossi, G., and Caucia, F. (1991) The crystal-chemistry of high-aluminium titanites. European Journal of Mineralogy, 3, 777–792.

Robbins, C.R. (1968) Synthetic $CaTiSiO_5$ and its germanium analogue. Materials Research Bulletin, 3, 693–698.

Salje, E., Schmidt, C., and Bismayer, U. (1993) Structural phase transition in titanite, $CaTiSiO_5$: A Ramanspectroscopic study. Physics and Chemistry of Minerals, 19, 502–506.

Sheldrick, G.M. (1997) SHELX97. University of Göttingen, Germany.

Speer, J.A. and Gibbs, G.V. (1976) The crystal structure of synthetic titanite, $CaTiOSiO_4$, and the domain textures of natural titanites. American Mineralogist, 61, 238–247.

Stoe and Cie GmbH (1996) X-RED, Data Reduction. Darmstadt, Germany.

Taylor, M. and Brown, G.E. (1976) High-temperature structural study of the $P2_1/a$ - A2/a phase transition in synthetic titanite, $CaTiSiO_5$. American Mineralogist, 61, 435–447.

Van Heurck, C., Van Tendeloo, G., Ghose, S., and Amelinckx, S. (1991) Paraelectric-antiferroelectric phase transition in titanite, $CaTiSiO_5$. II. Electron diffraction and electron microscopic studies of the transition dynamics. Physics and Chemistry of Minerals, 17, 604–610.

Zachariasen, W.H. (1930) The crystal structure of titanite. Zeitschrift für Kristallographie,73, 7–16.

Zhang, M., Salje, E.K.H., and Bismayer, U. (1997) Structural phase transition near 825 K in titanite: Evidence from infrared spectroscopic observations. American Mineralogist, 82, 30–35.

MANUSCRIPT RECEIVED MAY 27, 2004
MANUSCRIPT ACCEPTED DECEMBER 22, 2004
MANUSCRIPT HANDLED BY PETER BURNS